

WZ production beyond NLO for high- p_T observables

Francisco Campanario^{1,*} and Sebastian Sapeta^{2,†}

¹*Institute for Theoretical Physics, KIT, 76128 Karlsruhe, Germany.*

²*Institute for Particle Physics Phenomenology, Durham University, South Rd, Durham DH1 3LE, UK.*

We use the LoopSim and VBFNLO packages to investigate a merged sample of partonic events that is accurate at NLO in QCD simultaneously for the WZ and WZ+jet production processes. In certain regions of phase space such a procedure is expected to account for the dominant part of the NNLO QCD corrections to the WZ production process. For a number of commonly used experimental observables, we find that these corrections are substantial, in the 30 – 100% range and in some cases their inclusion can reduce scale uncertainties by a factor of two. As in the underlying VBFNLO calculations, we include the leptonic decays of the vector bosons and all off-shell and finite-width effects.

PACS numbers: 12.38.Bx, 13.85.-t, 14.70.Fm, 14.70.Hp

I. INTRODUCTION

The study of di-boson production processes at the LHC is important both to test the Standard Model (SM) and because they constitute relevant backgrounds to the beyond standard physics (BSM) searches. They are for example sensitive to tri-linear gauge couplings (TGC) fixed by the underlying electroweak gauge group in the SM. Any deviation in the values observed at experiments would indicate new physics effects. In particular, WZ production measurements [1, 2] are relevant to constrain the WWZ tri-linear coupling and to search for charged heavy bosons from BSM sector via Jacobian peaks [3–6].

To match the experimental accuracy, precise and reliable predictions beyond the leading order approximation are required. The next-to-leading order (NLO) QCD corrections for WZ production were computed in [7, 8] and turned out to be sizable. These large corrections are a well known fact for colorless production channels. At NLO QCD, new topologies and new partonic subprocesses appear, Fig. 1, e.g. those with a W or Z emitted from a jet or an initial-state parton. These new configurations can have partonic luminosities (e.g. qg) that are enhanced over those present at LO (e.g. $q\bar{q}$), which can lead to large corrections in differential distributions. They also permit soft or collinear bosons emissions from a quark which results in $\alpha_s \alpha_{EW}^2 \ln^2(p_{T,j}/m_V)$ enhancement for a number of observables.

At the next-to-next-to-leading order (NNLO) further new sub-processes and topologies, including those with soft and collinear bosons, start to contribute, Fig. 1, which might also lead to large corrections in some regions of phase space.¹

Therefore, using only the NLO results to compute the WZ backgrounds may lead to a misinterpretation of a

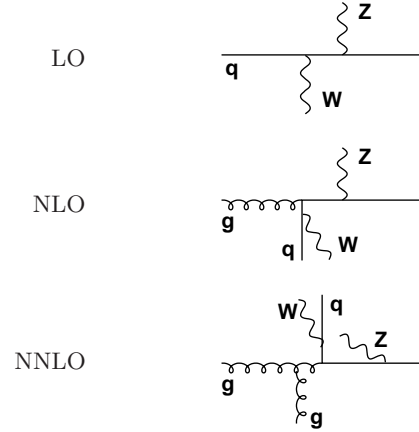


FIG. 1: Example diagram contributing to WZ production at LO, NLO and NNLO.

possible excess observed in data, which could be wrongly attributed to new physics. Thus, it is of great interest to try to assess the genuine NNLO QCD contributions for this process. The current state of the art is that the virtual two-loop corrections for WZ production are unknown. However, recently, the NLO QCD corrections for WZ+jet were computed in [10], including anomalous couplings [11], and they are available in the VBFNLO package [12]. This result provides the mixed real-virtual and the double real $\mathcal{O}(\alpha_s^2)$ contributions to the WZ production including the NLO corrections to the $q\bar{q}$ channel. This opens the possibility to merge the results for WZ@NLO² and WZj@NLO and obtain the part of the NNLO result for WZ production that is associated with channels absent at LO, which is the dominant contribution for a range of differential distributions at high p_T .

This can be done in a consistent way by employing the LoopSim method [13] which uses unitarity to cancel infrared and collinear divergences that arise when one

*Electronic address: francisco.campanario@kit.edu

†Electronic address: sebastian.sapeta@durham.ac.uk

¹We note that this was the case also for several observables in di-photon production [9].

²@ in e.g. WZ@NLO means NLO QCD corrections of WZ.

adds tree level results with different multiplicities. The LoopSim prescription is general and it has been found to work well for Z+jet and Drell-Yan production, especially for observables which receive significant corrections at NLO [13]. The method supplements a set of real and real-virtual diagrams with approximate contributions from loop diagrams. The result at a given order is denoted with \bar{n} to distinguish it from the exact result.

In this paper, we compute the \bar{n} NLO corrections (according to the notation introduced above) to WZ production at the LHC

$$pp \rightarrow W^\pm Z + X \rightarrow \ell_1^\pm \ell_1^{\pm(-)} \ell_2^+ \ell_2^- + X, \quad (1)$$

including the leptonic decays and full off-shell and finite width effects.

We organize this paper as follows: In Section II, we give technical details of our computation including a short description of the LoopSim method. In Section III, we present numerical results and the impact of the \bar{n} NLO QCD corrections on various differential distributions. In Section IV, we summarize our findings.

II. CALCULATIONAL DETAILS

For the calculation of WZ@ \bar{n} NLO, we used the implementations of WZ@NLO and WZj@NLO from the VBFNLO package [12], with the latter providing the double-real and the real-virtual parts of the NNLO result. Then the missing two-loop contributions are approximated by LoopSim from the tree-level and one-loop parts of WZj@NLO. To allow for communication between VBFNLO and LoopSim, we developed an interface between the two programs. On one hand, it consists of an extension of VBFNLO which enables it to write events in the Les Houches (LH) format at NLO and, on the other hand, of a class which reads the Les Houches events and passes them to LoopSim. Then LoopSim assigns an approximate angular-ordered branching structure to each LH event, with the help of the Cambridge/Aachen (C/A) [14, 15] jet algorithm. By default, it uses a radius $R_{LS} = 1$ and by varying R_{LS} , one probes one class of uncertainty of the method. As we shall see in the next section, except for the very low p_T region, this uncertainty is significantly smaller than that coming from renormalization and factorization scale variation.

The error that we make for an observable (A) is a finite constant associated with the LO topology and it is free of infrared and collinear divergences since these are, by construction, suitably treated by LoopSim. This implies

$$\sigma_{\bar{n}\text{NLO}}^{(A)} - \sigma_{\text{NNLO}}^{(A)} = \mathcal{O}\left(\alpha_s^2 \sigma_{\text{LO}}^{(A)}\right). \quad (2)$$

Thus, differential distributions sensitive to new channels and new kinematically enhanced configurations resulting in large NLO K-factors, should be close to the full NNLO result, providing predictions more precise than the pure NLO corrections to WZ.

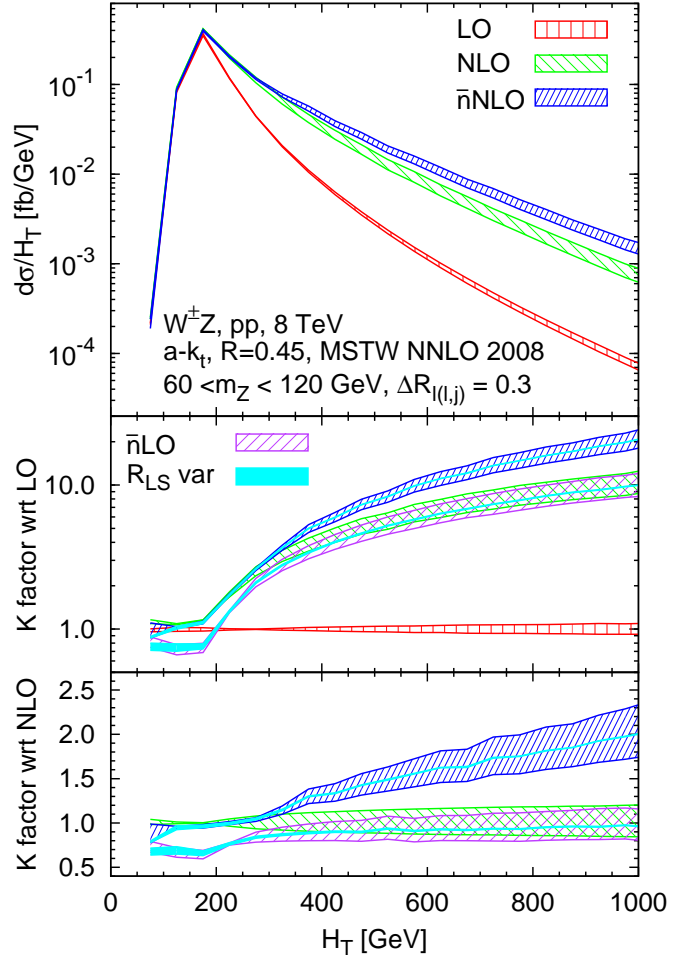


FIG. 2: Differential cross sections and K factors for the effective mass observable, defined in Eq. (4), for the LHC at $\sqrt{s} = 8$ TeV. The bands correspond to varying $\mu_F = \mu_R$ by factors 1/2 and 2 around the central value from Eq. (3). The cyan solid bands give the uncertainty related to the R_{LS} parameter varied between 0.5 and 1.5. The distribution is a sum of contributions from two unlike flavor decay channels, $e e \mu \nu_\mu$ and $\mu \mu e \nu_e$.

III. NUMERICAL RESULTS

In our computations, regardless of the order, we use the MSTW NNLO 2008 [16] PDFs with $\alpha_s(M_Z) = 0.11707$. We choose $m_Z = 91.1876$ GeV, $m_W = 80.398$ GeV and $G_F = 1.16637 \times 10^{-5} \text{ GeV}^{-2}$ as electroweak input parameters and derive the weak mixing angle from the Standard Model tree level relations. The center-of-mass energy is fixed to $\sqrt{s} = 8$ TeV if not specified otherwise. As in the underlying VBFNLO WZ@NLO and WZj@NLO calculations, only the channels with W and Z/ γ^* decaying into unlike flavor leptons are considered, i.e. $pp \rightarrow W^\pm Z + X \rightarrow \ell_1^\pm \ell_1^{\pm(-)} \ell_2^+ \ell_2^- + X$. From the theoretical perspective, to take into account all possible decay channels, i.e. $e e e \nu_e$, $e e \mu \nu_\mu$, $\mu \mu e \nu_e$, $\mu \mu \mu \nu_\mu$, one can safely multiply the single flavor result by a factor four,

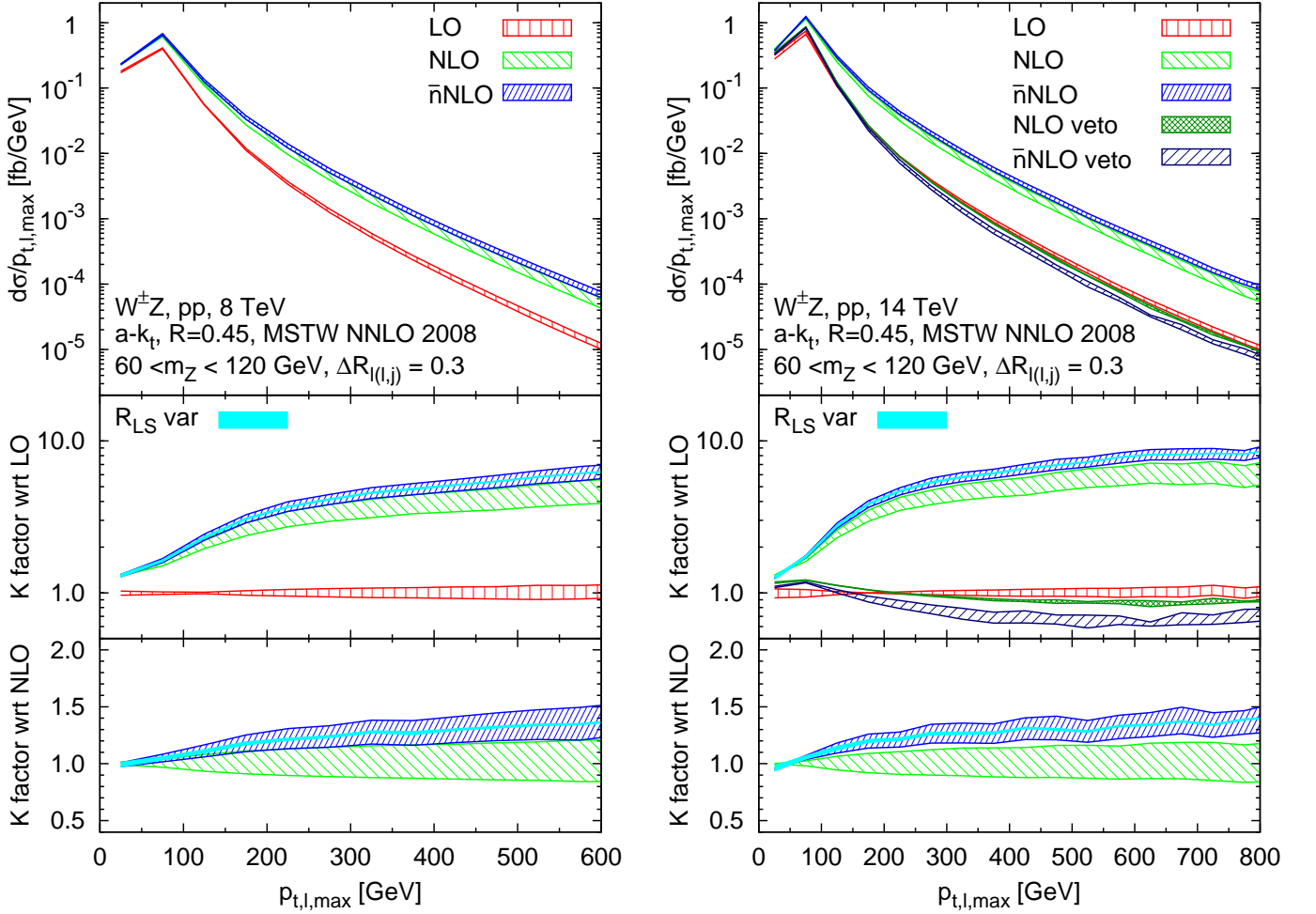


FIG. 3: Differential cross sections and K factors for the p_T of the hardest lepton for the LHC at $\sqrt{s} = 8$ TeV (left) and $\sqrt{s} = 14$ TeV (right). The bands correspond to varying $\mu_F = \mu_R$ by factors 1/2 and 2 around the central value from Eq. (3). The cyan solid bands give the uncertainty related to the R_{LS} parameter varied between 0.5 and 1.5. The distribution are sums of contributions from two unlike flavor decay channels, $ee\mu\nu_\mu$ and $\mu\mu e\nu_e$.

since the Fermi interferences due to identical particles in the final state are below per mille level [10]. However, as explained later, we shall only apply a cut on the reconstructed mass of the opposite charge same flavor lepton pair. Therefore, all the results shown in Figs. 2–4 correspond to the sum of contributions from the two decay channels, $ee\mu\nu_\mu$ and $\mu\mu e\nu_e$. All off-shell effects are included, which takes into account spin correlations and also virtual photons. Finite width effects, related to leptonic decays of the electroweak gauge bosons, are accounted for with a fixed-width scheme [10]. Top quark effects are not considered and all other quarks are taken massless. Effects from generation mixing are neglected since the CKM matrix is set to the identity matrix. As the central value for the factorization and renormalization scales we choose

$$\mu_{F,R} = \frac{1}{2} \sum p_{T,\text{partons}} + \frac{1}{2} \sqrt{p_{T,W}^2 + m_W^2} + \frac{1}{2} \sqrt{p_{T,Z}^2 + m_Z^2} \quad (3)$$

where $p_{T,V}$ and m_V have to be understood as the reconstructed transverse momenta and invariant masses of the decaying bosons. To study the impact of the QCD corrections, we choose inclusive cuts. The charged leptons are required to be hard and central: $p_{T,\ell} \geq 15(20)$, for l coming from $Z(W)$, and $|y_l| \leq 2.5$. The missing transverse energy must satisfy the cut $E_{T,\text{miss}} > 30$ GeV. The reconstructed mass from the opposite-charge same-flavor leptons has to lie in the window $60 < m_{l+l^-} < 120$ GeV, which also avoids singularities coming from off-shell photons, $\gamma^* \rightarrow \ell^+\ell^-$. We cluster all final state partons with $|y_p| \leq 5$ to jets with the anti- k_t algorithm [17], as implemented in FastJet [18, 19], with the radius $R = 0.45$. For observables that involve jets, we consider only those jets that lie in the rapidity range $|y_{\text{jet}}| \leq 4.5$ and have transverse momenta $p_{T,\text{jet}} \geq 30$ GeV. In addition, we impose a requirement on the lepton-lepton and lepton-jet separation in the azimuthal angle-rapidity plane $\Delta R_{l(l,j)} > 0.3$.

As a first check of our setup, we have merged WZ@LO and WZj@LO to produce WZ@ \bar{n} LO, which can be tested

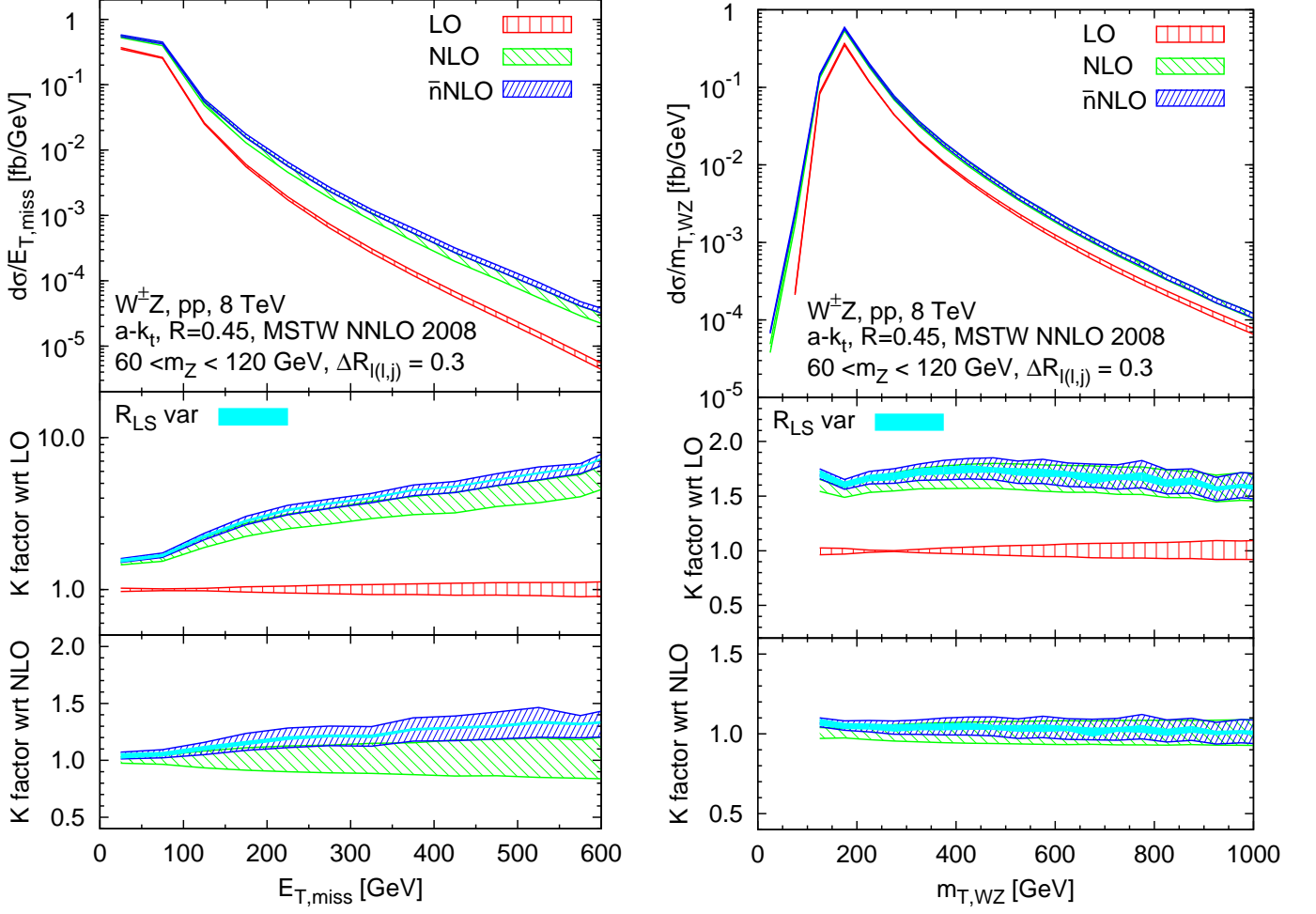


FIG. 4: Differential cross sections and K factors for the missing transverse energy (left) and the transverse mass of the WZ system (right) for the LHC at $\sqrt{s} = 8$ TeV. The bands correspond to varying $\mu_F = \mu_R$ by factors 1/2 and 2 around the central value from Eq. (3). The cyan solid bands give the uncertainty related to the R_{LS} parameter varied between 0.5 and 1.5. The distribution are sums of contributions from two unlike flavor decay channels, $ee\mu\nu_\mu$ and $\mu\mu\nu_e$.

against the full WZ@NLO result. In Fig. 2, we show the effective mass defined by

$$H_T = \sum p_{T,jets} + \sum p_{T,l} + E_{T,miss}, \quad (4)$$

which often enters in super-symmetry searches [20, 21]. This distribution is very sensitive to the enhancements from soft or collinear emissions of the electroweak bosons as well as to additional parton radiation coming from new channels.

In the middle panel of Fig. 2, we show the K factors with respect to the LO result and, in the bottom, the corresponding ratios to NLO. At low H_T values, the difference between \bar{n} LO and NLO is at the level of 30–40%. This is due to the fact that we do not have control over the finite virtual constant terms which are missing in our \bar{n} LO approximation. However, as the H_T increases, the \bar{n} LO result converges to the full NLO, providing a prediction more accurate than a simple LO calculation. Note in the middle panel the large \bar{n} LO corrections and fast

convergence to the NLO result, yielding K-factors of order of 10. The \bar{n} NLO corrections can be as large as 100% compared to NLO (bottom panel of Fig. 2) and they are clearly beyond the NLO scale uncertainties. We observe that the R_{LS} uncertainties are small and there is only a marginal reduction in the scale uncertainties at \bar{n} NLO. The latter is due to the fact that we are favoring regions of the phase space associated with new topologies entering at NNLO which are only computed at LO.

The integrated cross section for one lepton flavor, $\sigma(pp \rightarrow l_1\nu_{l_1}l_2l_2)$, dominated by the low H_T region, increases only by about 5% from 25.7 ± 1.0 (scale) fb at NLO to 26.9 ± 0.9 (scale) ± 0.4 (R_{LS}) fb at \bar{n} NLO. We have also computed the total cross sections for 7 TeV at NLO and the result agrees with this quoted in [2].

In Fig. 3, we show differential distributions for the lepton with maximum p_T for $\sqrt{s} = 8$ and $\sqrt{s} = 14$ TeV, left and right panels respectively. We observe that the \bar{n} NLO corrections are large at both energies. For the 14 TeV run, these corrections are beyond the renormal-

ization and factorization scale uncertainties above $p_T = 150$ GeV. The same is true for the 8 TeV case only at slightly higher p_T . Even though the effect is less pronounced than at 14 TeV, due to the smaller relative importance of additional parton radiation, the corrections are at the 15% level already at 200 GeV. In addition, for the 14 TeV case, we show the curves with a veto on the jets at NLO and \bar{n} NLO where we require the absence of any jets with $p_T > 50$ GeV. The \bar{n} NLO-veto corrections are negative and beyond the scale uncertainties of the NLO-vetoed predictions. This might be of relevance for anomalous coupling searches since vetoed distributions are often used to suppress additional radiation. The entire \bar{n} NLO-veto result has larger scale uncertainties than the NLO-vetoed curves, thus revealing, partially, accidental cancellation happening at NLO. Such a feature has been extensively discussed for jet vetoes also in the context of NNLO calculations of Higgs-boson production, e.g. [22] and references therein.

In Fig. 4 (left), we show the differential distributions for the missing transverse energy. We see that the \bar{n} NLO corrections to this observable can be as large as the 30%, exceeding the scale uncertainty of the NLO result. In the right-hand plot of Fig. 4, we show the cluster energy (transverse mass of the WZ system) defined by

$$m_{T,WZ} = \sqrt{(E_T^W + E_T^Z)^2 - (p_x^W + p_x^Z)^2 - (p_y^W + p_y^Z)^2}, \quad (5)$$

where $E_T^{W,Z}$ and $p_{x,y}^{W,Z}$ are the transverse energy and the transverse momentum components of the bosons reconstructed from the four-momenta of the leptons. The \bar{n} NLO corrections to this observable are small, which means that this distribution is not particularly sensitive to the new topologies that appear at NNLO. For the same reason, the finite terms from the two-loop diagrams, which are missing in the \bar{n} NLO result, are of larger relative importance for this observable than they are for H_T , $p_{T,l,\max}$ or $E_{T,\text{miss}}$, which is also reflected in larger R_{LS} uncertainties in the $m_{T,WZ}$ case.

The reason behind the marked difference in the relative size of the \bar{n} NLO corrections between $m_{T,WZ}$ and all the other observables which we have discussed is the following. For observables like $p_{T,l,\max}$ or $E_{T,\text{miss}}$, to

receive large contributions in the high- p_T region, it is enough that only one of the two bosons is produced at high p_T . This high- p_T boson recoils against a high- p_T QCD parton. The other boson can be in particular soft and collinear to a quark and such configurations, one of which is depicted in the bottom diagram of Fig. 1, come with the $\alpha_s^2 \alpha_{EW}^2 \ln^2(p_{T,j}/m_V)$ enhancement. In the case of $m_{T,WZ}$, however, the favored configurations are those in which both bosons have sizable p_T s and are preferably back to back therefore do not lead to logarithmic enhancements at NNLO.

IV. CONCLUSIONS

In this letter, we have used LoopSim together with VBFNLO to compute an approximation to the NNLO QCD corrections for the process $pp \rightarrow \ell_1^\pm \ell_2^\pm + X$. Our result, referred to as \bar{n} NLO, is expected to be accurate in the regions of phase space dominated by the topologies other than those present at LO. As in the underlying VBFNLO WZ@NLO and WZj@NLO calculations, our treatment includes the leptonic decays of the vector bosons and all off-shell and finite-width effects.

We found that the \bar{n} NLO corrections to a number of observables are sizable at high p_T and have non-trivial kinematic dependence. It is therefore important to take them into account in searches for physics beyond the SM and other physics analyses that involve WZ production. The VBFNLO+LoopSim code is available from the authors on request and it will be made public in the near future.

Acknowledgments

We thank Gavin Salam for collaboration during the initial stages of this work and for subsequent discussions and comments on the manuscript. FC acknowledges support by FEDER and Spanish MICINN under grant FPA2008-02878 and by the Deutsche Forschungsgemeinschaft under SFB TR-9 “Computergestützte Theoretische Teilchenphysik”. SS was in part supported by European Commission under contract PITN-GA-2010-264564.

-
- [1] G. Aad *et al.* [ATLAS Collaboration], arXiv:1208.1390 [hep-ex].
 - [2] [CMS Collaboration], CMS-PAS-EWK-11-010.
 - [3] G. Aad *et al.* [ATLAS Collaboration], Phys. Rev. D **85** (2012) 112012.
 - [4] [CMS Collaboration], CMS PAS EXO-11-095.
 - [5] J. Bagger, V. D. Barger, K. -m. Cheung, J. F. Gunion, T. Han, G. A. Ladinsky, R. Rosenfeld and C. P. Yuan, Phys. Rev. D **49** (1994) 1246 [hep-ph/9306256].
 - [6] C. Englert, B. Jager, M. Worek and D. Zeppenfeld, Phys. Rev. D **80** (2009) 035027 [arXiv:0810.4861 [hep-ph]].
 - [7] J. Ohnemus, Phys. Rev. D **44** (1991) 3477.
 - [8] S. Frixione, P. Nason and G. Ridolfi, Nucl. Phys. B **383** (1992) 3.
 - [9] S. Catani, L. Cieri, D. de Florian, G. Ferrera and M. Grazzini, Phys. Rev. Lett. **108** (2012) 072001.
 - [10] F. Campanario, C. Englert, S. Kallweit, M. Spannowsky and D. Zeppenfeld, JHEP **1007** (2010) 076.
 - [11] F. Campanario, C. Englert and M. Spannowsky, Phys. Rev. D **82** (2010) 054015.
 - [12] K. Arnold, J. Bellm, G. Bozzi, F. Campanario, C. Englert, B. Feigl, J. Frank and T. Figy *et al.*, arXiv:1207.4975 [hep-ph]; Comput. Phys. Commun. **180** (2009) 1661.

- [13] M. Rubin, G. P. Salam and S. Sapeta, JHEP **1009** (2010) 084.
- [14] Y. L. Dokshitzer, G. D. Leder, S. Moretti and B. R. Webber, JHEP **9708** (1997) 001 [arXiv:hep-ph/9707323].
- [15] M. Wobisch and T. Wengler, arXiv:hep-ph/9907280.
- [16] A. D. Martin, W. J. Stirling, R. S. Thorne and G. Watt, Eur. Phys. J. C **63** (2009) 189 [arXiv:0901.0002 [hep-ph]].
- [17] M. Cacciari, G. P. Salam and G. Soyez, JHEP **0804** (2008) 063 [arXiv:0802.1189 [hep-ph]].
- [18] M. Cacciari and G. P. Salam, Phys. Lett. B **641** (2006) 57 [hep-ph/0512210].
- [19] M. Cacciari, G. P. Salam and G. Soyez, <http://fastjet.fr/>.
- [20] [CMS Collaboration], CMS-PAS-SUS-12-017.
- [21] G. Aad *et al.* [ATLAS Collaboration], JHEP **1110** (2011) 107 [arXiv:1108.0366 [hep-ex]].
- [22] A. Banfi, G. P. Salam and G. Zanderighi, JHEP **1206** (2012) 159 [arXiv:1203.5773 [hep-ph]].